$CH_2Cl_2$–light petroleum ether had mp 159–161 °C.

*Anal.* Calcd for $C_{17}H_{24}O_2N_2S$ (320.45): C, 63.72; H, 7.55; N, 8.74. Found: C, 63.89; H, 7.44; N, 8.80.

**(+)-(5*R*)-*tert*-Butyl-1,3-cyclohexadiene (3).** To a suspension of 421 mg (1.31 mmol) of tosylhydrazone **16** in 1.5 mL of TMEDA was added at −62 °C with stirring 2.3 mL (3.9 mmol) of 1.7 M *n*-BuLi in hexane. The tosylhydrazone dissolved completely, and the solution became orange-brown. The reaction mixture was allowed to warm up to room temperature, stirred for an additional 1.5 h under $N_2$, and treated dropwise with 2 mL of $H_2O$. The almost colorless mixture was extracted with pentane, and the organic extracts were washed with $H_2O$, dried ($MgSO_4$), and filtered through 30 g of activity II basic alumina. The filtrate (50 mL), after 1:100 dilution with hexane, had $A = 0.605$ at 260 nm (1 cm), corresponding to a 54% yield of diene ($\epsilon_{261}$ 4311). The filtrate was concentrated by distillation, and the residue was distilled (kugelrohr) at 74–76 °C (50 mm). The diene (70 mg, 39% yield) was obtained as a colorless oil, 96% pure by analytical GC (columns A and B). Samples for spectroscopy were further purified by preparative GC (column E) to yield 7% of diene **3** of >99.5% purity. [Racemic diene has been reported previously[41] and had bp 45–49 °C (10 mm); UV $\epsilon_{259}$ 4021 (isooctane)]. Diene **7** had $[\alpha]^{25}_D$ +187°, $[\alpha]^{25}_{578}$ +195°, $[\alpha]^{25}_{546}$ +228°, $[\alpha]^{25}_{436}$ +433°, $[\alpha]^{25}_{365}$ +815° (*c* 0.63); UV $\epsilon_{261}$ 4311 (methylcyclohexane–isopentane, 4:1 v/v); CD, Table I; IR (neat) $\nu$ 3050, 2970, 2920, 2880, 2835, 1480, 1470, 1395, 1370, 735, 720, 670, 650 $cm^{-1}$; $^1H$ NMR and $^{13}C$ NMR, Table III; MS *m/z* (rel intensity) 136 [$M^+$], 121 (20%), 79 (100%) amu.

**(+)-(5*R*)-*tert*-Butyl-3-deuterio-1,3-cyclohexadiene (18).** The deuterated diene was prepared exactly as for its protio analog (**3**) by quenching with $D_2O$ instead of $H_2O$ (see also preparation of **17**). The purified material (GC, column E) had $[\alpha]^{25}_D$ +186°, $[\alpha]^{25}_{436}$ +431° (*c* 0.79); UV $\epsilon_{261}$ 4308 (methylcyclohexane–isopentane, 4:1 v/v); CD $\Delta\epsilon_{303} = 0$, $\Delta\epsilon_{273} = +3.00$, $\Delta\epsilon_{265} = +3.19$, $\Delta\epsilon_{234} = 0$, $\Delta\epsilon_{219} = -3.64$, $\Delta\epsilon_{209} = 0$ (methylcyclohexane–isopentane, 4:1 v/v); IR (neat) $\nu$ 3050, 2970, 2920, 2880, 2835, 2260 (C–D), 1475, 1395, 1360, 745, 625 $cm^{-1}$; $^1H$ NMR and $^{13}$NMR in Table III; MS *m/z* (rel intensity) 137 [$M^+$], 122 (18%), 80 (100%) amu.

**Computational Details.** Idealized geometries were used as in Figure 8. The STO-4G minimal basis set,[46] in conjunction with the unoptimized geometries used here, yielded the following SCF total energies in hartrees (1 hartree = 627.5 kcal/mol): B17, −154.0961; CHD, −230.6749; MCA, −269.5287; MCAR, −269.5211; MCE, −269.5303; MC1, −269.5000; MC2, −269.5340. Molecular orbitals were localized using the Foster–Boys–Coffey procedure.[14d] Computations were carried out in double precision on the IBM 3033 computer at the Northern Europe Computation Center at Lundtofte, Denmark, and on the IBM 370/145 system at Southern Illinois University at Edwardsville.

**Acknowledgment.** D.A.L., J.K.G., K.G., B.V.C., and J.L.C. thank the National Science Foundation for support of this work. T.D.B. and Aa.E.H. thank the Scientific Affairs Division of NATO for a grant in support of this work. Aa.E.H. thanks the Danish Natural Science Research Council for a travel grant. Additional support was provided to T.D.B. by the Office of Research and Projects of Southern Illinois University at Edwardsville. We wish to thank Drs. Lois Durham and C. S. Pak of Stanford University for their assistance in obtaining 360-MHz $^1H$ NMR spectra of dienes **1** and **17**, and Dr. Anthony Ribeiro for assistance with dienes **2** and **18**, all at the Stanford Magnetic Resonance Laboratory (NSF No. GP23633 and NIH No. RR00711). We also thank Dr. Jerome Gurst for a critical reading of the manuscript and for preparing a sample of diene **25** and providing us with its CD and UV spectra.

# Carbon-13 Exchange Maps for the Elucidation of Chemical Exchange Networks

**Y. Huang,[‡] S. Macura,[†] and R. R. Ernst***

*Contribution from the Laboratorium für Physikalische Chemie, Eidgenössische Technische Hochschule, 8092 Zürich, Switzerland.* *Received February 2, 1981*

**Abstract:** The application of two-dimensional carbon-13 NMR spectroscopy for the elucidation of chemical exchange networks is proposed. The utility of carbon-13 chemical exchange maps is demonstrated by application to systems involving conformational rearrangements, bond shifts, and solvation exchange processes.

## I. Introduction

Recently, two-dimensional (2D) NMR exchange spectroscopy has been introduced for the elucidation of molecular exchange processes.[1] It has been found that 2D exchange spectroscopy is of significance for the investigation of cross-relaxation,[2-6] as well as for the study of chemical exchange networks.[1,7] The analysis of complex processes is greatly facilitated by the recording of informative 2D exchange maps.

So far, all 2D exchange studies have been based on proton resonance spectroscopy.[1-8] It has, however, been found that homonuclear spin–spin couplings in systems of abundant spins can lead to undesirable features in a 2D exchange map. Whenever two nuclei are connected by a network of spin–spin couplings, so-called *J* cross-peaks may appear in the 2D exchange spectrum.[8] These peaks are caused by a coherent magnetization transfer through the spin–spin coupling network. The resulting cross-peaks may be misinterpreted as cross-relaxation or chemical exchange cross-peaks.

We propose here to utilize carbon-13 resonance for the recording of 2D exchange maps. For low abundance nuclei, complicating effects like *J* cross-peaks are completely absent. Each spin represents an ideal tracer which allows one to trail the exchange pathways.

[‡]Physics Department, Huadong Normal University, Shanghai, P.R. China.
[†]Academic Guest 1979–1980 from the Institute of Physical Chemistry, Faculty of Sciences, 11000 Beograd, Yugoslavia.

(1) J. Jeener, B. H. Meier, P. Bachmann, and R. R. Ernst, *J. Chem. Phys.*, **71**, 4546 (1979).
(2) S. Macura and R. R. Ernst, *Mol. Phys.*, **41**, 95 (1980).
(3) Anil Kumar, R. R. Ernst, and K. Wüthrich, *Biochem. Biophys. Res. Commun.*, **95**, 1 (1980).
(4) Anil Kumar, G. Wagner, R. R. Ernst, and K. Wüthrich, *Biochem. Biophys. Res. Commun.*, **96**, 1156 (1980).
(5) R. Baumann, Anil Kumar, R. R. Ernst, and K. Wüthrich, *J. Magn. Reson.*, in press.
(6) Anil Kumar, G. Wagner, R. R. Ernst, and K. Wüthrich, submitted for publication.
(7) B. H. Meier and R. R. Ernst, *J. Am. Chem. Soc.*, **101**, 6441 (1979).
(8) S. Macura, Y. Huang, D. Suter, and R. R. Ernst, *J. Magn. Reson.*, **43**, 259 (1981).

0002-7863/81/1503-5327$01.25/0 

It is well-known[9-17] that one-dimensional carbon-13 NMR spectroscopy is a valuable tool for the investigation of chemical exchange processes. Numerous exchange mechanisms have been clarified by $^{13}C$ NMR, including intramolecular rotation,[9] ring puckering,[10] bond shifts,[11] exchange in metal chelate complexes,[12] and ligand exchange and fluxional behavior in metal carbonyl complexes.[13-17]

Most investigations of chemical exchange have been based on an analysis of the exchange-broadened line shape.[18-20] In order to elucidate complex exchange networks, it is necessary to operate near coalescence where the line shape is most sensitive to the details of the exchange processes. However, for large chemical shift changes induced by the exchange reactions, the intensity of the exchange-broadened lines may become extremely weak. Examples are known where $^{13}C$ chemical shifts change by 30 ppm and more in the course of a chemical rearrangement. At 100 MHz $^{13}C$ resonance, a signal intensity reduction at coalescence by factors up to $10^4$ has to be expected in comparison with a nonexchanging carbon line. It is therefore often difficult or impossible to extract the desired line shape information with sufficient accuracy.[21]

In such situations, saturation transfer studies have proved to be more practical.[22,23] It is possible to work in the slow exchange temperature region and to obtain detailed information on exchange processes. Of particular use are time-resolved saturation transfer studies[10,24,25] in analogy to the measurement of transient nuclear Overhauser effects.[23,26-28] Saturation transfer studies, however, can be quite time consuming and demanding as each line has to be perturbed in turn while observing the response of all other lines. For closely spaced resonances a sufficiently selective perturbation of a single line may even be impossible.

2D chemical exchange spectroscopy is an almost ideal alternative to saturation transfer studies in the sense that all exchange pathways can be elucidated simultaneously by a simple and uncritical technique. It merely requires the application of nonselective radio frequency pulses. The magnetization components which are supposed to exchange are at first "frequency-labeled". After an exchange period of fixed length, the new locations of the exchanged magnetization components are determined. The frequency labels allow one to trace back the exchange pathways in arbitrarily complex exchange networks.

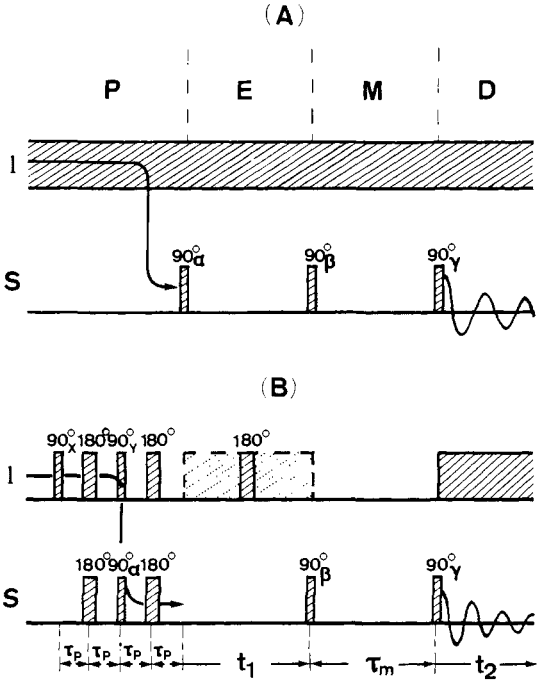


**Figure 1.** Experimental schemes of 2D carbon-13 chemical exchange spectroscopy. (A) Basic three-pulse sequence with simultaneous $I$ spin (proton) noise decoupling. $P$ = preparation period, $E$ = evolution period with time variable $t_1$, $M$ = mixing period of fixed duration $\tau_m$, $D$ = detection period with time variable $t_2$. In the most simple realization, the pulse phases $\alpha$, $\beta$, and $\gamma$ are equal. For the compensation of axial peaks and of transverse interference or for quadrature phase detection, several experiments with different pulse phases may be coadded. (B) Improved pulse sequence using polarization transfer via $J$ order (refocused INEPT) for the creation of initial carbon-13 ($S$ spin) coherence with $\tau_P = {}^1/_4J$. Proton decoupling during the evolution period may be effected by a 180° proton pulse or by noise decoupling.

In the next section, we discuss the methodological aspects of 2D carbon-13 chemical exchange spectroscopy. The technique is then demonstrated by means of three examples involving (a) chemical exchange by a ring puckering process, (b) exchange by Cope rearrangements, and (c) simultaneous solvation exchange and internal rotation.

## II. Methodological Aspects of 2D Carbon-13 Chemical Exchange Spectroscopy

The basic three-pulse sequence, used for 2D proton exchange spectroscopy[1,7] and visualized in Figure 1, can be applied without major modification also to $^{13}C$ resonance. After an initial 90° pulse, the magnetization components are precessing for a time $t_1$ to acquire their "frequency labels". A second 90° pulse rotates back the frequency-labeled magnetization components along the $z$ axis. It follows then an exchange period of length $\tau_m$. At the end of it, a third 90° pulse samples the exchanged magnetization components whose frequencies are measured during the final free precession period. For unique frequency labeling, the experiment has to be repeated for a set of equidistant $t_1$ values. The resulting two-dimensional set of data values is, finally, Fourier transformed in two dimensions.

Continuous proton noise decoupling[29] is normally applied during the evolution and detection periods to eliminate all heteronuclear spin–spin couplings. Although heteronuclear spin–spin couplings of rare nuclei do not lead to disturbing effects, such as $J$ cross-peaks,[8] their elimination is desirable to simplify the spectra in complete analogy to conventional one-dimensional spectra.

2D spectroscopy experiments are inherently quite time consuming, and it is necessary to minimize performance time by optimizing sensitivity. In the simplest case, the continuous proton irradiation transfers proton magnetization to the carbon-13 spins

(9) O. A. Gansow, J. Killough, and A. Burke, *J. Am. Chem. Soc.*, **93**, 4297 (1971).
(10) B. E. Mann, *J. Magn. Reson.*, **21**, 17 (1976); **25**, 91 (1977); P. Ahlberg, *Chem. Scr.*, **9**, 47 (1976).
(11) K. Lammertsma and H. Cerfontain, *J. Am. Chem. Soc.*, **101**, 3618 (1979).
(12) D. Doddrell and J. D. Roberts, *J. Am. Chem. Soc.*, **92**, 4484, 5255 (1970).
(13) O. A. Gansow, A. R. Burke, and W. D. Venon, *J. Am. Chem. Soc.*, **94**, 2550 (1972).
(14) F. A. Cotton, L. Kruczynski, B. L. Shapiro, and L. F. Johnson, *J. Am. Chem. Soc.*, **94**, 6191 (1972).
(15) L. T. Todd and J. R. Wilkinson, *J. Organomet. Chem.*, **77**, 1 (1974).
(16) M. H. Chisholm and S. Godleski, *Prog. Inorg. Chem.*, **20**, 299 (1974).
(17) H. W. Spiess, R. Grosescu, and U. Haeberlen, *Chem. Phys.*, **6**, 226 (1974).
(18) G. Binsch, *J. Am. Chem. Soc.*, **91**, 1304 (1969).
(19) L. M. Jackman and F. A. Cotton, "Dynamic Nuclear Magnetic Resonance Spectroscopy", Academic Press, New York, 1975.
(20) J. I. Kaplan and G. Fraenkel, "NMR of Chemically Exchanging Systems", Academic Press, New York, 1980.
(21) M. L. Martin, J.-J. Delpuech, and G. J. Martin, "Practical NMR Spectroscopy", Heyden, London, 1980, p 311.
(22) S. Forsen and R. A. Hoffman, *J. Chem. Phys.*, **40**, 1189 (1964); R. A. Hoffman and S. Forsen, *ibid.*, **45**, 2049 (1966).
(23) J. H. Noggle and R. E. Schirmer, "The Nuclear Overhauser Effect: Chemical Applications", Academic Press, New York, 1971.
(24) F. W. Dahlquist, K. J. Longmuir, and R. B. Duvernet, *J. Magn. Reson.*, **17**, 406 (1975).
(25) J. R. Alger and J. H. Prestegard, *J. Magn. Reson.*, **27**, 137 (1977).
(26) A. Kalk and H. J. C. Berendsen, *J. Magn. Reson.*, **24**, 343 (1976).
(27) S. L. Gordon and K. Wüthrich, *J. Am. Chem. Soc.*, **100**, 7094 (1978).
(28) G. Wagner and K. Wüthrich, *J. Magn. Reson.*, **33**, 675 (1979).
(29) R. R. Ernst, *J. Chem. Phys.*, **45**, 3845 (1966).

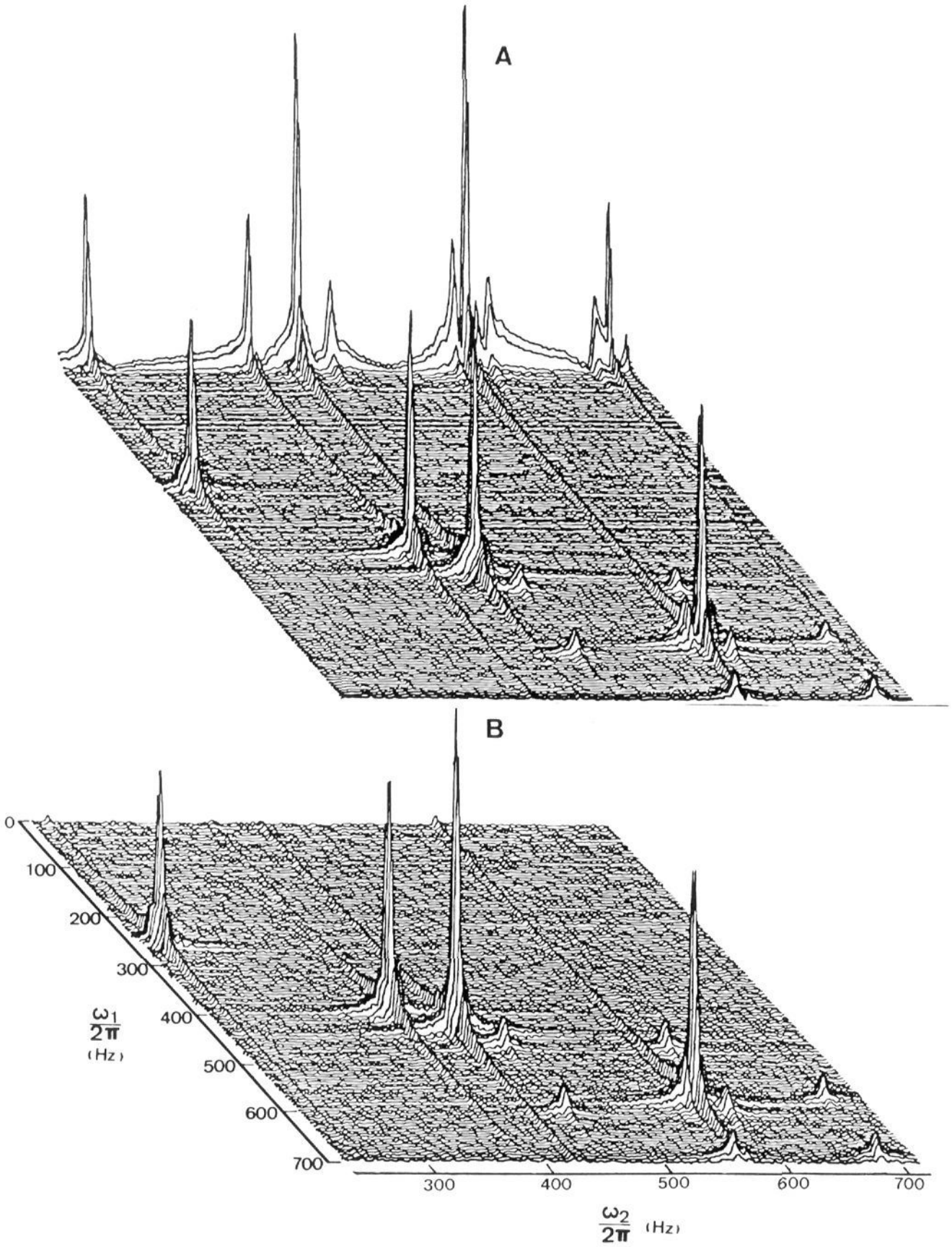


**Figure 2.** 2D 22.6 MHz carbon-13 exchange spectra of an equimolar mixture of *cis*- and *trans*-decalin to demonstrate the suppression of axial peaks. (A) Application of the basic three-pulse sequence with $\alpha = \beta = \gamma = 0°$ (cf. Figure 1A). (B) Coaddition of the results of two experiments with $\alpha = \beta = \gamma = 0°$ and $\alpha = 180°$, $\beta = 0°$, $\gamma = 180°$ for the suppression of axial peaks and of transverse interference. The slow exchange 2D spectra were recorded at 238 K. Toluene-$d_8$ (20 vol %) was used for the field frequency lock. The mixing time $\tau_m$ was fixed at 0.5 s. For each of the 128 $t_1$ values ranging from 0 to 76.8 ms 16 scans were coadded. Each FID was represented by 512 digitized samples. A 256 by 1024 data matrix was Fourier transformed in two dimensions. Absolute value spectra are plotted.

via the nuclear Overhauser effect (Figure 1A). The recently developed pulsed magnetization transfer experiments[30-36] are often superior to transfer via nuclear Overhauser effect. They create maximum initial $^{13}C$ magnetization and minimize the experiment time by increasing the magnetization transfer rate. Pulsed coherence transfer schemes are particularly efficient for systems with short proton and long carbon-13 relaxation times. One may also consider the addition of relaxation agents to further shorten the repetition-rate-limiting proton relaxation time.

We have successfully applied to scheme indicated in Figure 1B. Proton magnetization is transferred by a pulse sequence via a *J*-ordered state[33,36,37] to the carbon-13 spins. This scheme, proposed by Burum and Ernst, can be called refocused INEPT.[36] It represents an improvement of the INEPT technique introduced for magnetization transfer by Morris and Freeman.[34,35] It is often necessary to minimize the proton decoupling power to avoid excessive sample heating. For this purpose, proton decoupling during the evolution period may be effected by a single 180° pulse. To avoid incomplete decoupling in the presence of strong proton–proton couplings, it is preferable to apply noise decoupling during evolution and detection periods. During the mixing period, however, proton decoupling is unnecessary.

(30) A. A. Maudsley and R. R. Ernst, *Chem. Phys. Lett.*, **50**, 368 (1977).
(31) A. A. Maudsley, L. Müller, and R. R. Ernst, *J. Magn. Reson.*, **28**, 463 (1977).
(32) R. D. Bertrand, W. B. Moniz, A. N. Garroway, and G. C. Chingas, *J. Am. Chem. Soc.*, **100**, 5227 (1978).
(33) G. C. Chingas, A. N. Garroway, W. B. Moniz, and R. D. Bertrand, *J. Am. Chem. Soc.*, **102**, 2526 (1980); A. N. Garroway and G. C. Chingas, *J. Magn. Reson.*, **38**, 179 (1980).
(34) G. A. Morris and R. Freeman, *J. Am. Chem. Soc.*, **101**, 760 (1979).
(35) G. A. Morris, *J. Am. Chem. Soc.*, **102**, 428 (1980).
(36) D. P. Burum and R. R. Ernst, *J. Magn. Reson.*, **39**, 163 (1980).
(37) K. J. Packer and K. M. Wright, *J. Magn. Reson.*, **41**, 268 (1980).

The suppression of the axial peaks, which appear in a 2D exchange spectrum along the axis $\omega_1 = 0$ (Figure 2A) is of considerable importance. They may be quite strong and are accompanied by long tails extending parallel to the $\omega_1$ axis through the entire 2D spectrum. Axial peaks originate from longitudinal magnetization without frequency labeling which recovered from zero during an extended mixing period and is converted into transverse magnetization by the third radio frequence pulse. By coaddition of the responses to two phase-shifted pulse sequences it is possible to selectively suppress axial peaks. It has been suggested in ref 2 to apply in successive experiments the following two pulse sequences: (1) $\alpha = 0°$, $\beta = 0°$, $\gamma = 0°$, and (2) $\alpha = 180°$, $\beta = 0°$, $\gamma = 180°$. The result of such an experiment is shown in Figure 2B. The axial peaks have been eliminated almost completely. The weak remaining ridges are caused by long-term spectrometer instability which leads to bands of so-called "$t_1$ noise". The dual experiment indicated above eliminates, at the same time, the effects of transverse interference.[2]

The experimental results presented in this paper have been obtained on a homemade spectrometer equipped with a 2.114 T Bruker electromagnet and a Varian 620/L-100 computer with Diablo 43 disk unit. Single-phase detection has been employed. For quadrature phase detection in both frequency domains, additional phase-shifted experiments would have to be included to permit the distinction of all four quadrants.[38]

## III. Ring Puckering in Decalin

It is well-known[39-41] that *cis*-decalin has two energetically equivalent chair–chair conformations (cf. Figure 3B). A dynamic exchange process interconverts the two conformations. *cis*-Decalin contains five pairs of equivalent carbon nuclei, [1,5], [2,6], [3,7], [4,8], and [9,10]. The chair–chair conversion permutes [1,5] and [4,8] as well as [2,6] and [3,7] while the pair [9,10] remains unaffected. The thermodynamic parameters governing the conformational change have been measured by Dalling et al.:[41] $\Delta G^{\ddagger} = 52.8$ kJ/mol, $\Delta H^{\ddagger} = 56.9 \pm 3$ kJ/mol.

*trans*-Decaline, on the other hand, has only one minimum energy chair–chair conformation and, therefore, appears stereochemically rigid. It contains three groups of equivalent carbon nuclei, [1,5,4,8], [2,6,3,7], and [9,10].

Figures 2 and 3 show 2D chemical exchange spectra and 2D chemical exchange maps of an equimolar mixture of *cis*- and *trans*-decalin for three temperatures. The low-temperature spectra of Figures 2 and 3A, recorded at 241 K, contain all the expected peaks. Along the principal diagonal, we find the auto-peaks of the five nonequivalent carbon pairs of *cis*-decalin and the three peaks of *trans*-decalin. In addition, there are two pairs of cross-peaks which identify the pairs of exchanging carbon nuclei in *cis*-decalin.

The 2D exchange map of Figure 3B has been recorded at the coalescence temperature of 273 K and shows exclusively the auto-peaks of the nonexchanging carbon resonances while the resonances of exchanging nuclei are broadened to such an extent that their intensities disappear in the background noise.

The exchange map of Figure 3C, recorded at 299 K, shows six auto-peaks, three peaks for *trans*-decalin and three peaks for *cis*-decalin. It represents a high-temperature spectrum in the fast-exchange regime. The two peaks of *cis*-decalin affected by exchange exhibit still some exchange broadening which is apparent from the reduced signal amplitude.

The series of exchange maps of Figure 3 clearly demonstrates that the slow-exchange region is most informative. The intensities of the exchange cross-peaks allow the determination of the exchange pathways and an estimation of the corresponding exchange rate constants. Near coalescence and, in the fast exchange limit, 2D spectroscopy do not provide additional information on the exchange process which could not be obtained from a one-dimensional spectrum.

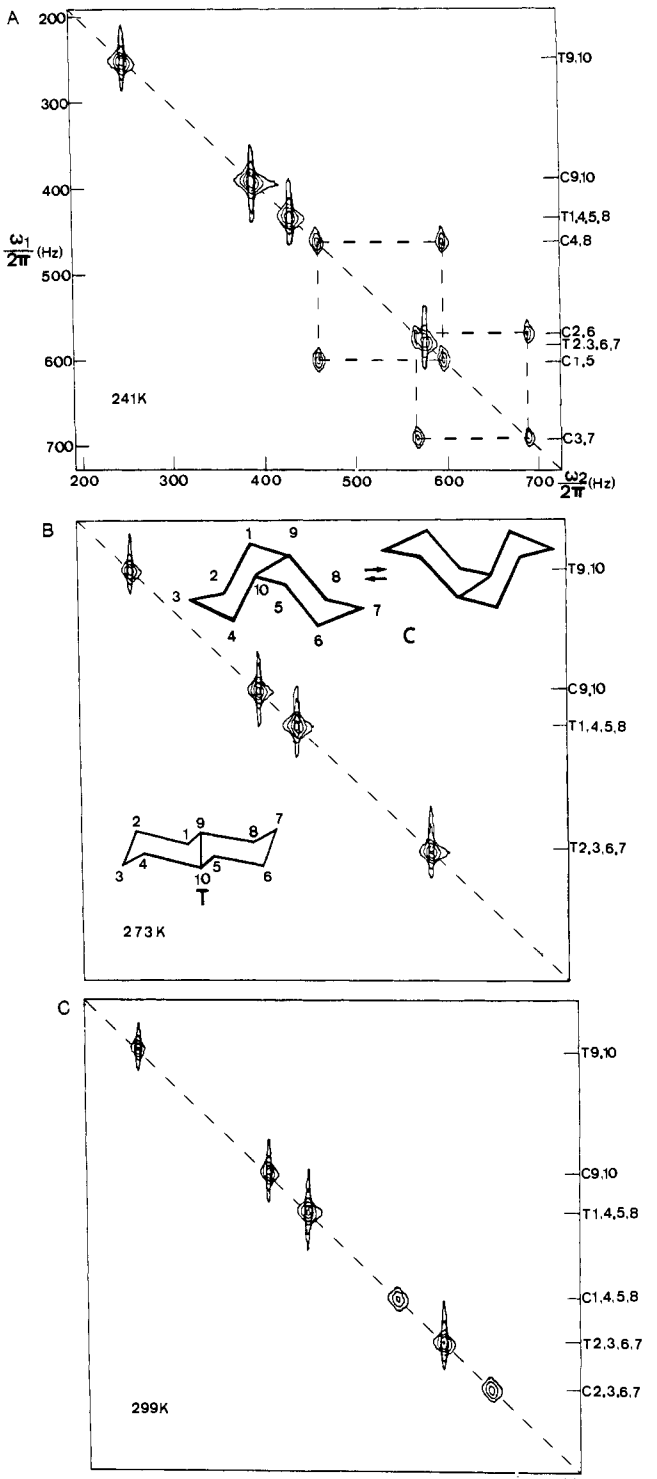


**Figure 3.** Carbon-13 exchange maps for a mixture of *cis*-decalin (C) and *trans*-decalin (T) at three different temperatures. 30 vol % methylene-$d_2$ chloride has been added for the field-frequency lock. (A) Low-temperature, slow-exchange map at 241 K. The map has been recorded under conditions comparable to those of the 2D spectra of Figure 2. (B) Exchange map recorded at the coalescence temperature of 273 K. (C) High-temperature, fast-exchange map at 299 K. The mixing time was fixed in all examples at 0.5 s. Eight FID's have been coadded for each of the 128 $t_1$ values from 0 to 76.8 ms. A 256 by 1024 data matrix has been Fourier transformed in two dimensions and plotted by a contour plot program.[1] The assignments of the signal peaks are indicated.

## IV. Bond Shift in Bullvalene

By numerous experimental studies, it has been shown that bullvalene exhibits a complicated network of Cope rearrange-

(38) R. R. Ernst, W. P. Aue, P. Bachmann, J. Karhan, Anil Kumar, and L. Müller, *Proc. Ampere Int. Summer Sch., 4th*, **1976**, 89 (1976).
(39) J. Dale, *Top. Stereochem.*, **9**, 258 (1976).
(40) F. R. Jensen and B. H. Beck, *Tetrahedron Lett.*, 4523 (1966).
(41) D. K. Dalling, D. M. Grant, and L. F. Johnson, *J. Am. Chem. Soc.*, **93**, 3678 (1971).

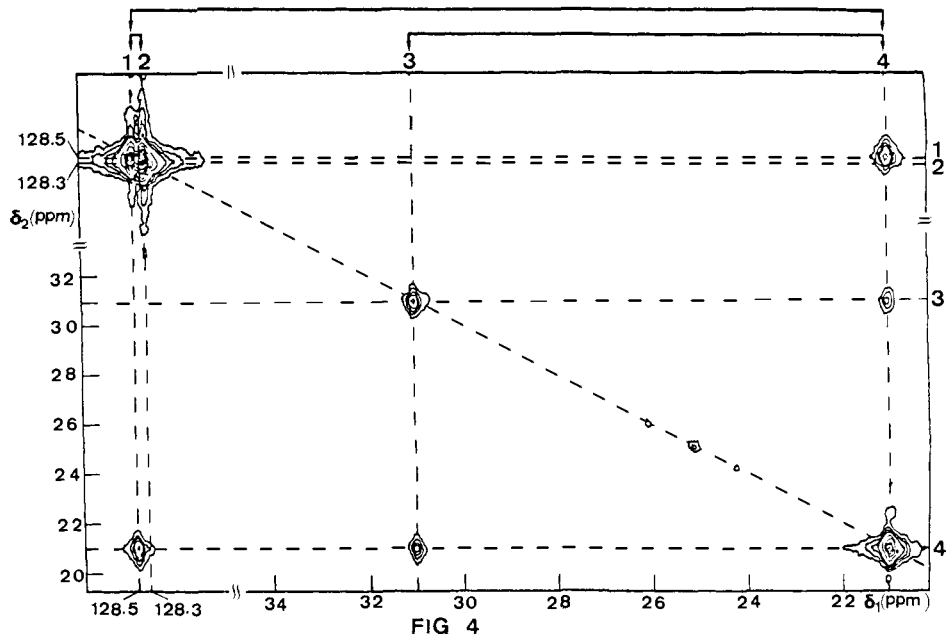


FIG 4

**Figure 4.** 22.6 MHz carbon-13 exchange map of 70 mg of bullvalene dissolved in a 2:1 mixture of tetrahydrofuran-$d_8$ and carbon disulfide recorded at 213 K. Mixing time: 0.5 s. Sixteen pairs of FID's, using the phase-alternated pulse sequence described in section II, were coadded for each of the 512 $t_1$ values from 0 to 256 ms. A 1024 by 2048 data matrix was submitted to a 2D Fourier transformation and plotted by a contour plot program.[1] Besides the auto- and cross-peaks for the four groups of equivalent carbons, the map contains three auto-peaks which belong to the solvent tetrahydrofurane-$d_8$. Multiple frequency folding has been used to enhance the digital resolution of the spectrum. The succession of the bullvalene lines corresponds to reality, not however their apparent frequency separation. The solvent lines would occur normally outside of the bullvalene spectrum. The ppm scale indicates peak positions relative to $Me_4Si$.

ments.[42-46] From the NMR standpoint, bullvalene contains four classes of equivalent carbon nuclei, labeled 1–4, with populations 3, 3, 1, and 3, respectively: The four classes of carbon nuclei

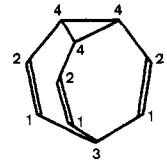


are connected by the following exchange network[46] with the rate

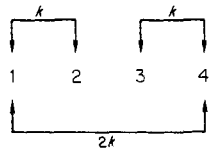


constants $k$ and $2k$. It leads to a system of kinetic equations for the exchange of magnetization between the four sites:

$$\begin{bmatrix} \dot{M}_1 \\ \dot{M}_2 \\ \dot{M}_3 \\ \dot{M}_4 \end{bmatrix} = k \underbrace{\begin{bmatrix} -3 & 1 & 0 & 2 \\ 1 & -1 & 0 & 0 \\ 0 & 0 & -3 & 1 \\ 2 & 0 & 3 & -3 \end{bmatrix}}_{\mathbf{K}} \times \begin{bmatrix} M_1 \\ M_2 \\ M_3 \\ M_4 \end{bmatrix} \qquad (1)$$

with the kinetic matrix **K**.

The cross-peak intensities in a 2D exchange map recorded for sufficiently short mixing time $\tau_m$ are proportional to the rates of exchange $E_{kl}$ between the classes of equivalent nuclei. The 2D exchange map, therefore, gives directly the exchange rate matrix **E** (rather than the kinetic matrix **K**). For bullvalene, we find the exchange rate matrix

$$\mathbf{E} = k[A_{Bullv}]_0 \begin{bmatrix} -9 & 3 & 0 & 6 \\ 3 & -3 & 0 & 0 \\ 0 & 0 & -3 & 3 \\ 6 & 0 & 3 & -9 \end{bmatrix} \qquad (2)$$

The rate constants $K_{kl}$ contained in the kinetic matrix **K** can be calculated from the experimental exchange rates $E_{kl}$ by division of each column $l$ of **E** by the corresponding equilibrium concentration $[A_l]_0$ of site $l$,

$$K_{kl} = E_{kl}/[A_l]_0 \qquad (3)$$

The principle of microscopic reversibility leads invariably to a symmetric matrix **E** and to a symmetric 2D exchange map, although the kinetic matrix **K** may be asymmetric, as for example in eq 1.

Figure 4 shows a 2D chemical exchange map of bullvalene recorded at 223 K with a 2:1 mixture of tetrahydrofurane-$d_8$ and carbon disulfide as solvent. Along the principal diagonal, we find the four auto-peaks corresponding to the four groups of equivalent carbons with the expected intensity ratios 3:3:1:3. The chemical shifts of the olefinic carbons 1 and 2 are rather similar.

According to the exchange rate matrix, eq 2, we expect three pairs of cross-peaks, two pairs of equal and one with double intensity. The expected intensity ratio 2:1 of the cross-peaks (1,4), (4,1) and (3,4), (4,3) is visible. On the other hand, the two cross-peaks (1,2) and (2,1) are not fully resolved in this survey spectrum and would require a blow up for a detailed analysis. In addition, we find on the principal diagonal the three central peaks of the 1 2 3 2 1 quintet of the solvent tetrahydrofurane-$d_8$. Naturally, there are no cross-peaks which relate solvent and solute resonances.

The exchange map of Figure 4 visualizes the relevant information on the exchange network, information which otherwise would have to be deduced by tedious saturation transfer experiments or by critical line shape analysis near the coalescence temperature where the signal peak intensities are very low.[46] Analysis of the line shape near coalescence is not easy, in this case,

(42) W. von E. Doerig and W. R. Roth, *Tetrahedron*, **19**, 715 (1963).
(43) M. Saunders, *Tetrahedron Lett.*, 1699 (1963).
(44) A. Allerhand and H. S. Gutowsky, *J. Am. Chem. Soc.*, **87**, 4092 (1965).
(45) J. D. Graham and E. R. Santee, *J. Am. Chem. Soc.*, **88**, 3453 (1966).
(46) J. F. M. Oth, K. Müllen, J.-M. Gilles, and G. Schröder, *Helv. Chim. Acta*, **57**, 1415 (1974).

because of the large line widths in the coalescence temperature region.

## V. Dynamics of Solvation of $Al^{3+}$ in Dimethylformamide Water Mixture

It has been found by proton NMR measurements[47,48] that *N,N*-dimethylformamide (DMF) forms in an aqueous solution of $AlCl_3$ a long-lived solvation complex with the six-coordinated ion $Al^{3+}$. The exchange between bulk and solvation water is fast and leads to a single water resonance. However, separate proton and carbon resonance signals can be observed for bulk and complexed DMF, indicating slow exchange between the two environments.[47] In addition, DMF is capable of hindered internal rotation which interchanges the two nonequivalent methyl groups. The question arises whether it is possible to visualize these two independent processes by 2D exchange maps.

Figure 5A represents the $^{13}C$ exchange map at 313 K. At this temperature, the internal rotation about the C–N bond in DMF is expected to be very slow as the barrier of rotation is rather high with $\Delta G^{\ddagger} = 87.5$ kJ/mol and $\Delta H^{\ddagger} = 85.8$ kJ/mol.[49] Correspondingly, no cross-peaks are visible between the two nonequivalent methyl groups $CH_3(A)$ and $CH_3(B)$. However, Figure 5A demonstrates that at room temperature the exchange rate between solvated and free DMF is sufficiently high that within the 0.2 s mixing time an appreciable exchange takes place. This process explains the three pairs of off-diagonal peaks for the $CH_3(A)$, $CH_3(B)$, and CHO carbon-13 spins. Solvation changes the chemical shifts of $CH_3(A)$ and $CH_3(B)$ by 2.5 and 2.4 ppm, respectively, while the chemical shift of the formic carbon changes by 0.7 ppm only.

Solvation has a marked effect on the line width of the formic carbon resonance which increases, probably due to interaction with the aluminum spin $I = {}^5/_2$. Nevertheless, the two cross-peaks of the formic carbon are clearly visible. Indeed, they are stronger than the auto-peak of the complexed formic carbon. For sites with equal line width and equal population, cross-peak intensities cannot surpass those of the auto-peaks. However, for sites with unequal line width or unequal population, cross-peaks can be more intense than the weaker of the two corresponding auto-peaks.

We note in Figure 5A one, yet unexplained, auto-peak at 32.8 ppm. Its intensity depends on the preparation of the sample and increases with the age of the solution. It can be identified as the methyl carbon resonance of *N,N*-dimethylamine. This molecule results from the acid-catalyzed hydrolysis of DMF in the $AlCl_3$ solution. This process is accelerated at higher temperature.

The exchange map of Figure 5B demonstrates the exchange phenomena at 349 K. This temperature is above the coalescence temperature of the solvation exchange process and each of the two methyl groups is represented by a single broadened auto-peak on the principal diagonal. The formic carbon produces a single narrow peak. At this elevated temperature, we find now a pair of cross-peaks between the two methyl resonances. It indicates the onset of internal rotation about the C–N bond. The cross-peak intensity allows an estimate of the exchange lifetime at 349 K to ~0.8 s. The narrow *N,N*-dimethylamine peak has become the strongest peak of the entire spectrum, indicating an enhanced hydrolysis rate at 349 K.

## VI. Conclusions

Carbon-13 chemical exchange maps offer a valuable new possibility for the investigation of chemical exchange networks. The potential fields of application are numerous, extending from the investigation of conformational changes in organic molecules to dynamics in metal organic complexes and to exchange processes in biological macromolecules.

The application of carbon-13 resonance for 2D chemical exchange studies is advantageous for the absence of complications

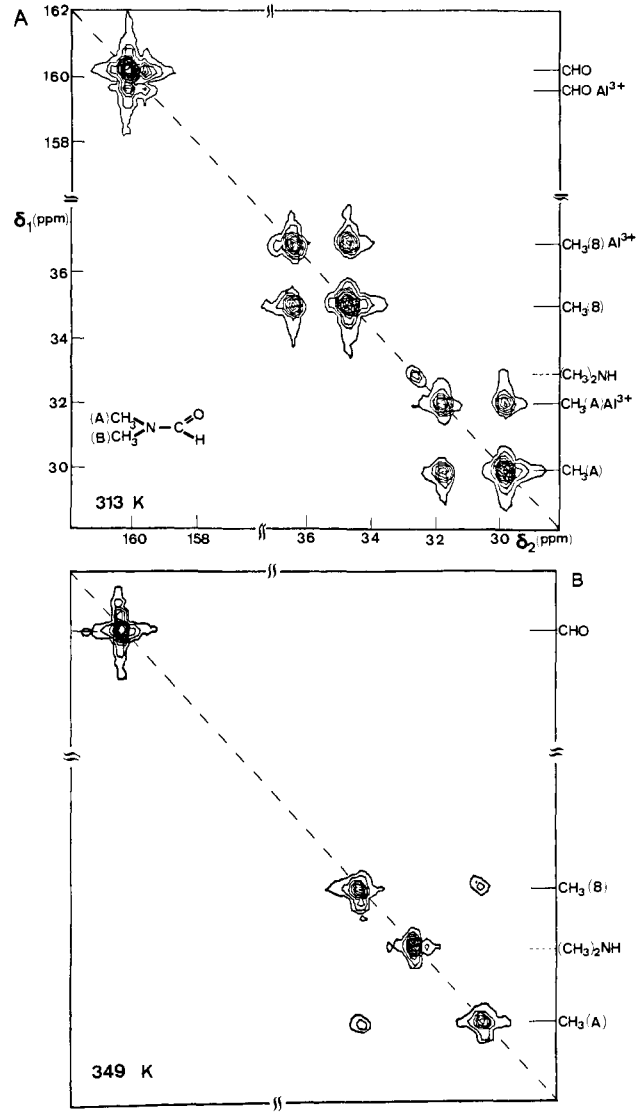


**Figure 5.** 22.6 MHz carbon-13 exchange maps of a saturated solution of $AlCl_3$ in a 4:1 mixture of *N,N*-dimethylformamide and $D_2O$. (A) Low-temperature, slow-exchange map recorded at 40 °C with a 0.2 s mixing time. Cross-peaks indicate slow exchange between solvated and free *N,N*-dimethylformamide molecules. (B) High-temperature exchange map recorded at 76 °C with 0.4 s mixing time. Cross-peaks indicate slow internal rotation about the C–N bond in *N,N*-dimethylformamide. 32 FID's have been coadded for each of the 512 $t_1$ values ranging from 0 to 128 ms. A 1024 by 1024 data matrix has been Fourier transformed in two dimensions. Frequency folding has been used to enhance the digital resolution of the 2D exchange map. The ppm scale indicates peak positions relative to $Me_4Si$.

caused by homonuclear spin–spin couplings which would lead to *J* cross-peaks. In addition, carbon-13 relaxation times are normally considerably longer than those of protons. Carbon-13 spins have therefore a longer lasting memory and permit the investigation of slower exchange processes which require long mixing times.

Analogous experiments are also feasible in the solid state in connection with magic angle sample spinning. The recent development of low-temperature magic-angle spinners[50,51] is of particular interest in this regard as it opens possibilities for investigating dynamic processes in solid state over a wide temperature range.

2D exchange maps are particularly well suited for a qualitative visualization of exchange networks. The recording of a single 2D

(47) A. Fratiello and D. P. Miller, *Mol. Phys.*, **11**, 37 (1966).
(48) A. Fratiello, R. E. Lee, V. M. Nishida, and R. E. Schuster, *J. Chem. Phys.*, **47**, 4951 (1967).
(49) T. Drakenberg, K.-I. Dahlquist, and S. Forsen, *J. Phys. Chem.*, **76**, 2178 (1972).
(50) C. A. Fyfe, J. R. Lyerla, and C. S. Yannoni, *J. Am. Chem. Soc.*, **100**, 5635 (1978).
(51) J. R. Lyerla, C. A. Fyfe, and C. S. Yannoni, *J. Am. Chem. Soc.*, **101**, 1351 (1979).

exchange map is often sufficient to obtain an order of magnitude indication of the involved exchange rates. The examples in this paper have been restricted to such a qualitative analysis. However, for a more quantitative determination of the rate constants, several exchange maps for different mixing times $\tau_m$ must be recorded. Of particular interest is the build-up of the cross-peak intensities for short mixing times in analogy to the determination of the nuclear Overhauser effect build-up rates.[6,27,28] It directly provides the individual rate constants.

Although 2D experiments are in general time consuming it should be remembered that thanks to the two-dimensional signal-averaging feature inherent in the 2D Fourier transformation a sensitivity not much lower than that in a one-dimensional spectrum recorded in the same total time can be achieved.[52]

**Acknowledgment.** Y.H. and S.M. acknowledge the receipt of grants for postdoctoral fellowships by the Swiss Federal Institute of Technology and by the Research Fund of S. R. Serbia, Yugoslavia, respectively. This research has been supported in part by the Swiss National Science Foundation. The authors are grateful to M. Linder and B. H. Meier for support and advice with regard to software for two-dimensional spectroscopy. The manuscript has been typed by Miss I. Müller. The authors gratefully acknowledge the receipt of a sample of bullvalene by Dr. J. Heinzer and Professor K. Müllen.

(52) W. P. Aue, P. Bachmann, A. Wokaun, and R. R. Ernst, *J. Magn. Reson.*, **29**, 523 (1978).

# The Importance of Hydrophobic–Hydrophilic Factors in Binding of Charged Substrates to Micelles: The Use of Extramicellar Probe Luminescence to Monitor Association of Cations to the Micelle

**Thomas K. Foreman, Warren M. Sobol, and David G. Whitten***

*Contribution from the Department of Chemistry, University of North Carolina, Chapel Hill, North Carolina 27514.* *Received December 15, 1980. Revised Manuscript Received April 23, 1981*

**Abstract:** The anionic metal complex **1**, $RuL_3^{4-}$, where L = 4,4′-dicarboxy-2,2′-bipyridine, has been used as an extramicellar luminescent probe to monitor the binding capacity of anionic sodium dodecylsulfate micelles for the quencher $Cu^{2+}$ and several organic cations. Addition of surfactant attenuates the quenching activity of the cations toward **1** in each case. For $Cu^{2+}$ the binding capacity, as monitored by the quenching of the extramicellar probe, is in good agreement with those determined for $Cu^{2+}$ and other divalent metal ions, using quite different methods; curvature in the quenching plot as $[Cu^{2+}]$ increases is attributed to screening of the micellar charge by bound $Cu^{2+}$. For $MV^{2+}$ quite different behavior is observed; the Stern–Volmer type quenching plot shows two good linear portions at any surfactant concentration. The portion with low slope at low $[MV^{2+}]$ is attributed to $MV^{2+}$ binding to the organized surfactant; at higher $[MV^{2+}]$ the steeper plot has a slope essentially the same as that obtained in water in the absence of micelles. The absence of curvature suggests association of several $MV^{2+}$ molecules does not inhibit binding of additional quenchers until nearly all the binding sites are occupied. This finding, combined with the relatively high binding capacity in terms of cation/SDS for $MV^{2+}$ compared to metal ions, suggests that $MV^{2+}$ binds at different sites and that other factors control its binding. Similar results have been obtained with other organic cations. The results are most consistent with a model whereby these bind at hydrocarbon–water interfaces and not primarily with the micelle head groups.

The surge of recent interest in chemical reactions occurring in organized assemblies such as micelles and vesicles has led to several investigations and some controversy concerning the nature, site, and extent of binding of various substrates with the assemblies.[2-5] Certainly one of the key features responsible for the numerous current studies of micellar phenomena is the remarkable ability of charged micelles to solubilize and concentrate a wide variety of reagents ranging from oppositely charged metal ions to hydrocarbons. Several investigations have established binding constants for different species; there have also been attempts to determine the limits to which a given substrate can bind or be solubilized. Studies with nonpolar solubilizates such as benzene and some aliphatic hydrocarbons, for example, indicate that in excess of 1 mol of substrate/mol of surfactant can be solubilized, in some cases without producing large effects on such micellar properties as the degree of aggregation or viscosity.[4,6-12] On the other hand, studies with uni- and divalent metal ions suggest many fewer than one ion/surfactant molecule can be accommodated.[13-17]

(1) Photochemical Reactivity in Organized Assemblies. 19. Paper 18: Schmehl, R. H.; Whitesell, L. G.; Whitten, D. G. *J. Am. Chem. Soc.*, in press.
(2) For recent reviews, see: Mittal, K. L., Ed. "Micellization, Solubilization and Microemulstions", Plenum: New York, 1977; Vol. I and II and ref 3–5.
(3) Mittal, K. L., Ed. "Solution Chemistry of Surfactants"; Plenum: New York, 1979.
(4) Menger, F. M. *Acc. Chem. Res.* **1979**, *12*, 111.
(5) Fendler, J. H.; Fendler, E. J. "Catalysis in Micellar and Macromolecular Systems"; Academic Press: New York, 1975.
(6) Mukerjee, P. "Solution Chemistry of Surfactants", Mittal, K. L., Ed.; Plenum: New York, 1979; pp 153–174.
(7) Bansal, K. M.; Patterson, L. K.; Fendler, E. J.; Fendler, J. H. *Int. J. Radiat. Phys. Chem.* **1971**, *3*, 321.
(8) Mukerjee, P.; Cardinal, J. R.; Desai, N. R. "Micellization, Solubilization and Microemulsions", Mittal, K. L., Ed.; Plenum: New York, 1977; p 241.
(9) Smith, M. B.; Alexander, A. E. *Proc. Int. Cong. Surf. Act., 2nd* **1957**, *1*, 311.
(10) Eriksson, J. C.; Gillberg, G. *Acta Chem. Scand.* **1966**, 20, 2019.
(11) McBain, M. E. L.; Hutchinson, E. "Solubilization and Related Phenomena"; Academic Press: New York, 1955.
(12) Elworthy, P. H.; Florence, A. T.; McFarlane, C. B. "Solubilization by Surface Active Agents and Its Application in Chemistry and the Biological Sciences"; Chapman and Hall: London, 1968.
(13) Fischer, M.; Knoche, W.; Fletcher, P. D. I.; Robinson, B. H.; White, N. C. *Colloid Polym. Sci.* **1980**, *258*, 733.
(14) Grätzel, M.; Thomas, J. K. *J. Phys. Chem.* **1974**, *78*, 2248.

0002-7863/81/1503-5333$01.25/0 